ChemComm

COMMUNICATION

View Article Online
View Journal | View Issue

Cite this: *Chem. Commun.*, 2022, **58**, 3138

Received 23rd December 2021,
Accepted 7th February 2022

DOI: 10.1039/d1cc07206d

rsc.li/chemcomm

Host–guest chemistry under confinement: peeking at early self-assembly events†

Roelof Steeno,[a] Andrea Minoia,[b] Roberto Lazzaroni,[b] Kunal S. Mali *[a] and Steven De Feyter *[a]

Nanoscopic lateral confinement created on a graphite surface enabled the study of embryonic stages of molecular self-assembly on solid surfaces using scanning tunneling microscopy performed at the solution/solid interface.

Molecular self-assembly on solid surfaces is a promising method for making defined two-dimensional (2D) structures. It enables precise spatial control over the deposition of chemical functionality at the nanoscale. This research area has witnessed rapid progress due to the fundamental interest in understanding how supramolecular and interfacial interactions influence the arrangement of molecules on solid surfaces. A variety of structurally diverse supramolecular architectures ranging from simple lamellar networks to intricate rosettes, and from nanoporous monolayers to hierarchically complex multicomponent structures have been reported.[1–3]

Despite several sophisticated designs published to date, it remains challenging to predict the morphology of the network based on the molecular structure. Unravelling the mechanisms that lead to crystalline monolayers *via* stepwise evolution from single molecule adsorption and through subsequent self-assembly steps is key to achieving such predictive power. A major bottleneck in this pursuit is the moderate temporal resolution of standard scanning tunnelling microscopy (STM), a technique predominantly used for characterizing physisorbed self-assembled networks at the solution/solid interface.[4–7] While STM offers extremely high spatial resolution, its moderate time resolution means that the nucleation and growth processes, which are central to understanding the assembly mechanism, are not captured. Furthermore, due to the scarcity of alternative/complementary analytical techniques that are sensitive enough to characterize monolayers formed at the solution/solid interface, little is known about the embryonic stages of the assembly process.[8–10]

Fast scanning STM is one of the obvious solutions. However, very few[11] commercial options exist. Moreover, maintaining high resolution, while scanning fast, remains a challenge. Standard STM, which typically requires tens of seconds to a few minutes for acquiring a single image, allows 'snapshots' of processes to be captured. While the nucleation and free growth are too fast to be captured, the coarsening of domains is readily observed.[12]

Using the moderate temporal resolution of standard STM setup, incorporation dynamics of coronene in nanoporous host networks has been studied. The guest was added to preformed host networks. The onset of occupation of the host cavities was then monitored.[13] This study provided important information on the time scale of guest incorporation into a preformed host network. However, the host and the guest molecules are often deposited simultaneously and thus the information on the early self-assembly events is lost. Such information has broad implications in sectors where molecular self-assembly is used as a bottom-up fabrication strategy.[14]

In this work, we use lateral nanoconfinement to access early stages of self-assembly by studying a host–guest system made up of 5-octadecyloxy-isophthalic acid (ISAOC18) and coronene (COR)[15] inside nanometer thick, shallow nanocompartments created by carving out an organic layer covalently bound to the basal plane of highly oriented pyrolytic graphite (HOPG) using STM based nanolithography, hereon referred to as nanoshaving.[16] The adsorption and self-assembly of the building blocks inside the nanocorrals coupled with the act of nanoshaving itself allowed us to observe liquid-like structures which represent the embryonic stages of network formation that are otherwise not captured in standard STM experiments. The experimental results have been supported by rigorous molecular mechanics (MM) and molecular dynamics (MD) simulations, which not only provide important insight into the relative stabilization energies of the host–guest networks

[a] *Division of Molecular Imaging and Photonics, Department of Chemistry, KU Leuven, Celestijnenlaan 200F, B-3001 Leuven, Belgium. E-mail: kunal.mali@kuleuven.be, steven.defeyter@kuleuven.be*

[b] *Laboratory for Chemistry of Novel Materials, Materials Research Institute, University of Mons, Place du Parc 20, 7000 Mons, Belgium*

† Electronic supplementary information (ESI) available. See DOI: 10.1039/d1cc07206d

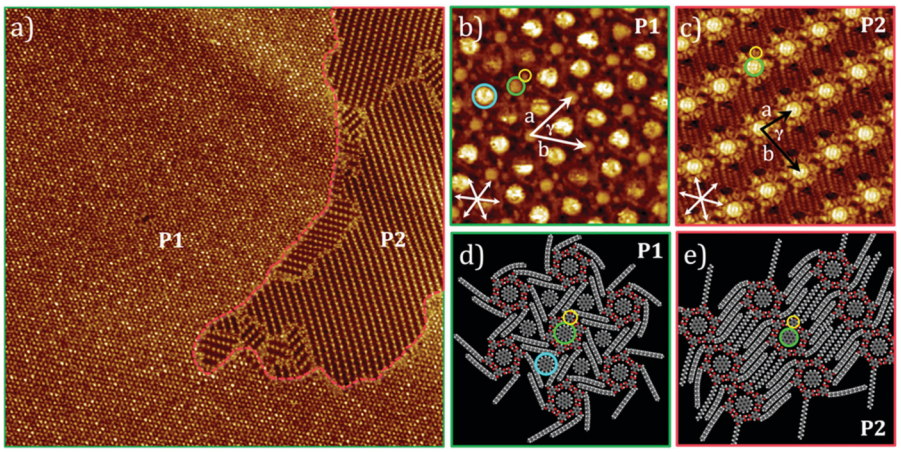

Fig. 1 (a) Large-scale STM image (200 × 200 nm^2) showing two different COR/ISAOC18 polymorphs (**P1** and **P2**) formed at the pristine HOPG/1-PO interface (C_{ISA} = 0.3 mM, C_{COR} = 0.5 mM). High-resolution STM images of polymorphs **P1** (b) and **P2** (c) and the corresponding molecular models (d and e). Scan size (b and c) = 16 × 16 nm^2. The coloured circles highlight the constituent building blocks (green = COR in hexagonal cavity, cyan = COR in triangular cavity, yellow = ISA headgroup). Imaging conditions: (a) V_{bias} = −0.50 V, I_{set} = 50 pA (b) V_{bias} = −0.65 V, I_{set} = 50 pA, (c) V_{bias} = −0.62 V, I_{set} = 50 pA.

but also reveal pathways that lead to the formation of the different polymorphs. The fundamental knowledge obtained from the experiments and simulations was then used to select a given polymorph by controlling the amount of dominant partner in the assembly process or by altering the degree of confinement.

Prior to studying the COR–ISAOC18 host–guest system under nanoconfinement, it was thoroughly screened for the presence of any unknown polymorphs. This led to the discovery of a new polymorph (**P2**) in addition to the previously reported[15] one (**P1**). Fig. 1 shows the STM images of two polymorphs formed at the 1-phenyloctane (1-PO)/HOPG interface upon deposition of a solution containing the two building blocks. The primary assembling motif for both **P1** and **P2** consists of a COR molecule immobilized by a hydrogen-bonded hexamer of ISAOC18.

The polymorphs differ from each other in two aspects: First is the way the alkoxy chains are packed surrounding the central host–guest cluster. MM simulations (Section B1 in the ESI†) indicate that for **P1**, they form propeller shaped arrangement *via* an acute bend near oxygen atom leading to the formation of a Kagomé type network. The peripheral triangular cavities also each contain a COR molecule (Fig. 1b and d). The COR in triangular cavities appear bigger and brighter compared to COR in the hexagonal cavities. This could be related to dimer formation facilitated by the perpendicular orientation of the alkyl chains with respect to HOPG (Section B2 in the ESI†). For **P2**, the chains interdigitate to form a columnar packing (Fig. 1c and e). The second difference is the stoichiometry of the two components. The **P1** unit cell consists of 3 COR and 6 ISAOC18 molecules whereas for **P2** this number is 1 and 6, respectively. **P1** thus contains a factor ∼2.2 more COR per nm^2 compared to **P2**, whereas a factor ∼0.7 less ISAOC18 per nm^2. MM/MD simulations indicate that the stabilization energy per unit area for **P2** is higher than that of **P1** (Table 1), which was further validated by annealing experiments (Section B3 in ESI†).

Table 1 Unit cell parameters and stabilization energies per unit area of the two polymorphs (see ESI for E_{sta} calculations)

	Unit cell (exp)			Unit cell (calc)			
	a (nm)	b (nm)	γ (°)	a (nm)	b (nm)	γ (°)	E_{sta} (kcal mol^{-1} nm^{-2})
P1	4.1 ± 0.1	4.0 ± 0.2	58.6 ± 3.1	4.1	4.0	61	−27.8
P2	4.0 ± 0.1	2.7 ± 0.1	78.2 ± 1.5	4.3	2.7	82	−39.5

Lateral nanoconfinement on the HOPG surface was created as reported previously.[16] Briefly, the surface bound aryl groups were removed using the STM tip by scanning the surface at high tunnelling currents in the presence of 1-PO solution of COR and ISAOC18 (Fig. 2a and b). Square-shaped pristine graphite areas (50 × 50 nm^2), which serve as nanocompartments for confinement experiments, were created *via* nanoshaving. Since nanoshaving was carried out in the presence of COR/ISAOC18 solution, the physisorption and the self-assembly occurs in concert with nanoshaving as the surface of pristine graphite becomes available with each scanned line (Fig. 2b). Subsequent STM imaging revealed that the nanocorrals were filled with small domains of **P1** (green, Fig. 2c) and **P2** (red, Fig. 2c). Surrounding these crystalline domains, a semi-ordered organization of circular features was observed. Based on the size and shape, we conclude that these are COR molecules.

The small **P1** and **P2** domains that nucleated immediately after nanoshaving either grew slowly and filled the corrals or slowly disappeared. The nucleation and subsequent growth/disappearance of the polymorphs could be followed in detail with STM imaging (Section B4 in ESI†). Fig. 2d shows the STM image of the same nanocorral as in Fig. 2c but imaged after 85 minutes. It clearly demonstrates how slowly the two known polymorphs grow at the expense of the initially adsorbed COR. Furthermore, high-resolution imaging of the

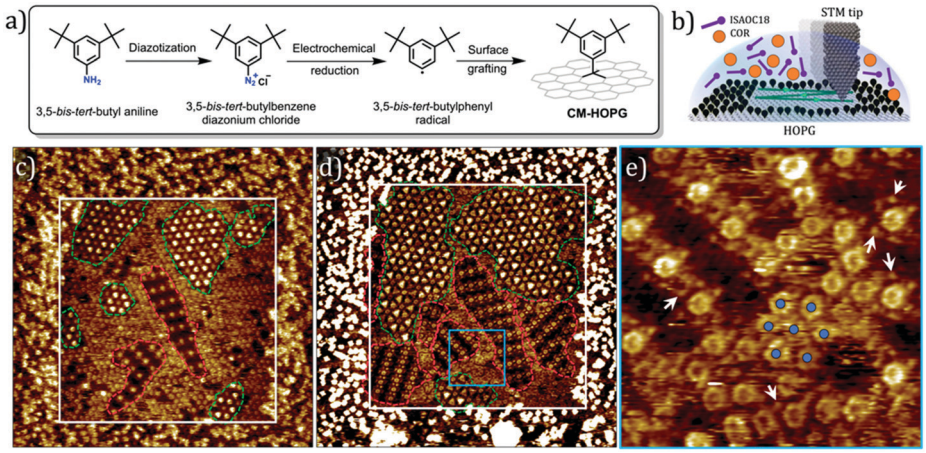

Fig. 2 (a) Functionalization of the graphite surface. (b) Schematic of the nanoshaving process. (c) STM image (100 × 100 nm^2) showing the nucleation of domains of **P1** (green) and **P2** (red) polymorphs under confinement. The surrounding area is filled with blob-like semi-ordered features. (d) Same nanocorral as in (c) imaged after 85 minutes. (e) Magnified area (15 × 15 nm^2) from (d, blue square) showing immobilized COR molecules (blue circles) plausibly spaced apart by co-adsorbed ISA headgroups (white arrows) (C_{ISA} = C_{COR} = 0.5 mM). Imaging conditions: V_{bias} = −0.90 V, I_{set} = 50 pA.

COR-based domains (blue circles, Fig. 2e) revealed that the center-to-center spacing between adjacent COR molecules is ∼1.7 nm.

This is too large to account for close-packed COR assembly where a spacing of ∼1.1 nm is expected.[17,18] The self-assembly of COR by itself at the solution–graphite interface has never been reported to the best of our knowledge. When the confinement experiments were carried out using only COR in 1-PO, no assembly was detected inside corrals (Section B5 in the ESI†) indicating that COR domains may not be solely composed of COR. STM images show features (white arrows, Fig. 2e) surrounding the COR which could be the ISA headgroups.

To shed more light into the experimental observations, MM/MD simulations were carried out (Section B6 in ESI†). MM simulations revealed that COR has higher adsorption energy *per* unit area (E_{ads} = −34.7 kcal mol^{-1} nm^{-2}) than ISAOC18 (E_{ads} = −31.3 kcal mol^{-1} nm^{-2}) and is poorly solvated (E_{solv} = −103.7 kcal mol^{-1}) in 1-PO compared to ISAOC18 (E_{solv} = −163 kcal mol^{-1}). This implies that given the higher flexibility of ISAOC18, the former could desorb relatively easily, either partially or completely from the surface compared to COR, which would 'stick' to the surface better than ISAOC18.

To further confirm the stronger adsorption of COR relative to ISAOC18, MD simulations were performed. A system composed of COR and ISAOC18 molecules adsorbed on graphite (treated as a rigid body) and "wetted" with solvent molecules was investigated (Section B6 in the ESI†). Despite the presence of the solvent, coronene molecules never desorb, while ISAOC18 molecules could be seen leaving the surface and entering the liquid phase (Fig. 3a), even at room temperature. The MM/MD simulations combined with the confinement experiments thus confirm the stronger and faster adsorption of COR relative to ISAOC18. MD simulations carried out on assemblies containing equal number of COR and ISAOC18 molecules confined within a small area revealed the formation of aggregates that resemble the final **P1** and **P2** motifs. Within

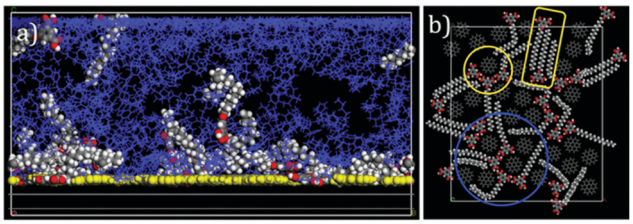

Fig. 3 (a) Snapshot of an MD run after 500 ps at 600 K for 28 COR (yellow), 24 ISAOC18 and 261 1-PO (blue) molecules on HOPG (grey horizontal line). (b) MD snapshot showing the evolution of **P1**- (yellow circle) and **P2**-like (yellow rectangle) structures. The blue circle highlights a less ordered region where the mean COR–COR distance is 1.5–1.7 nm.

these nuclei, COR–COR separations of 1.5–1.7 nm were found (blue circle, Fig. 3b), which agrees well with the STM data (Fig. 2e). The simulations further suggest that the COR clusters nucleated immediately after nanoshaving likely contain ISAOC18 embedded in between COR molecules. These 'embryos' are plausibly the kinetic structures from which the nucleation of **P1** and **P2** begins. Last but not the least, by changing the relative number of COR and ISAOC18 molecules included in the MD simulations, it was possible to observe a preference of **P1**-like and **P2**-like structures at high and low COR content, respectively (see Section B7 in ESI†).

These results indicate that the fast and stronger adsorption of COR determines the fate of the self-assembly. Thus, it should be possible to select between the two polymorphs by (i) changing the amount of COR in the solution and (ii) by controlling the amounts of COR that gets to nucleate on the surface. To this end, network formation from a range of different COR/ISAOC18 mole ratios was studied and percentage surface coverage (θ) of each polymorph was estimated. Fig. 4a shows that **P1** is preferentially (∼95%) formed at high (1.7) mole ratio. Intermediate mole ratios (0.6–1) yielded near equal surface coverage for **P1** and **P2** whereas at low mole ratio (0.1), predominantly **P2**

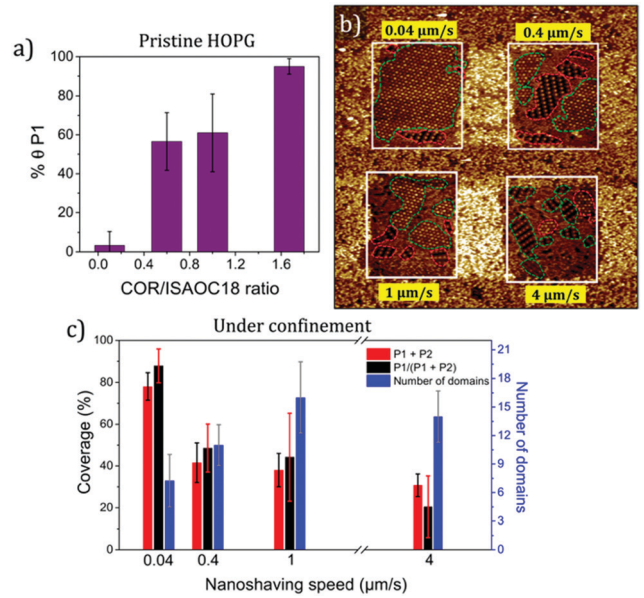

Fig. 4 (a) Percentage surface coverage (% θ) of **P1** as a function of COR/ISAOC18 mole ratio. (b) STM image (150 × 150 nm^2) showing the effect of nanoshaving speed on the occupation of corrals (50 × 50 nm^2) by **P1** (green) and **P2** (red) domains. (C_{ISA} = 0.5 mM, C_{COR} = 0.3 mM). (c) Surface coverage *versus* scan speed from four separate experiments.

(~97%) was observed. Further evidence of the vital role played by COR adsorption in the early stages was found by comparing the time taken by **P1** and **P2** to fill up the corrals entirely as a function of mole ratio (see Section B8 in ESI†). At a low mole ratio (0.1) **P2** domains immediately filled up the corrals completely. For intermediate (0.6) and high (1–1.67) ratios, it took a few minutes to several tens of minutes, respectively to fill the corral with **P1** and **P2** (see Fig. S8 and Videos in the ESI†), suggesting that an increase in the COR content reduces the rates of **P1** and **P2** nucleation.

The selection of **P1** could also be achieved under nanoconfinement by simply controlling the nanoshaving speed. Since COR adsorbs strongly compared to ISAOC18 which is more prone to desorption, limiting the space available for self-assembly could increase the possibility of COR occupation. This may lead to a local increase in COR concentration and therefore favour the formation of **P1**. Higher degree of confinement achieved at early stages by slow nanoshaving could thus promote **P1**. This hypothesis is based on our previous work where a narrow nanoshaved channel could bias the formation of a metastable polymorph.[16] Fig. 4b and c clearly show that reduction in the nanoshaving speed leads to an increase in the surface coverage of **P1**. The total coverage of **P1** and **P2** domains increased from 40% to 80% accompanied with a decrease in the number of domains. This indicates that the exposure of the first few graphite nanochannels upon nanoshaving occurs on a timescale of the nucleation of **P1**. Further corral extension thus allows growth of the domains instead of additional nucleation.

In conclusion, confinement created by STM-based lithography enabled the study of the embryonic stages of molecular self-assembly which are otherwise not accessible under standard experimental conditions. By combining STM results with MM/MD simulations we could identify the dominant partner in a host–guest system. This knowledge proved to be useful for polymorph selection by controlling the amount of fast-nucleating and strongly-adsorbing component, both on pristine surfaces and under confinement.

The authors acknowledge financial support from the Fund of Scientific Research Flanders (FWO), KU Leuven – Internal Funds. This work was in part supported by FWO and FNRS under EOS 30489208. The molecular modelling activities are supported by FNRS (Consortium des Équipements de Calcul Intensif – CÉCI, under Grant 2.5020.11) and by the Walloon Region (ZENOBE Tier-1 supercomputer, under grant 1117545).

Conflicts of interest

There are no conflicts to declare.

Notes and references

1 C. R. Pfeiffer, N. Pearce and N. R. Champness, *Chem. Commun.*, 2017, **53**, 11528–11539.
2 K. S. Mali, N. Pearce, S. De Feyter and N. R. Champness, *Chem. Soc. Rev.*, 2017, **46**, 2520–2542.
3 D. P. Goronzy, M. Ebrahimi, F. Rosei, A. Arramel, Y. Fang, S. De Feyter, S. L. Tait, C. Wang, P. H. Beton, A. T. S. Wee, P. S. Weiss and D. F. Perepichka, *ACS Nano*, 2018, **12**, 7445–7481.
4 A. G. Slater, L. M. A. Perdigão, P. H. Beton and N. R. Champness, *Acc. Chem. Res.*, 2014, **47**, 3417–3427.
5 A. G. Slater, P. H. Beton and N. R. Champness, *Chem. Sci.*, 2011, **2**, 1440–1448.
6 A. Ciesielski, C.-A. Palma, M. Bonini and P. Samorì, *Adv. Mater.*, 2010, **22**, 3506–3520.
7 M. Lackinger and W. M. Heckl, *Langmuir*, 2009, **25**, 11307–11321.
8 P. N. Nirmalraj, D. Thompson and H. E. Riel, *Sci. Rep.*, 2015, **5**, 10116.
9 K. W. Hipps and U. Mazur, *Langmuir*, 2018, **34**, 3–17.
10 C.-A. Palma, M. Cecchini and P. Samori, *Chem. Soc. Rev.*, 2012, **41**, 3713–3730.
11 C. Dri, M. Panighel, D. Tiemann, L. L. Patera, G. Troiano, Y. Fukamori, F. Knoller, B. A. J. Lechner, G. Cautero, D. Giuressi, G. Comelli, J. Fraxedas, C. Africh and F. Esch, *Ultramicroscopy*, 2019, **205**, 49–56.
12 S. De Feyter, H. Xu and K. Mali, *Chimia*, 2012, **66**, 38–43.
13 G. Eder, S. Kloft, N. Martsinovich, K. Mahata, M. Schmittel, W. M. Heckl and M. Lackinger, *Langmuir*, 2011, **27**, 13563–13571.
14 M. Gobbi, E. Orgiu and P. Samorì, *Adv. Mater.*, 2018, **30**, 1706103.
15 K. W. Park, J. Adisoejoso, J. Plas, J. Hong, K. Müllen and S. De Feyter, *Langmuir*, 2014, **30**, 15206–15211.
16 A. M. Bragança, A. Minoia, R. Steeno, J. Seibel, B. E. Hirsch, L. Verstraete, O. Ivasenko, K. Müllen, K. S. Mali, R. Lazzaroni and S. De Feyter, *J. Am. Chem. Soc.*, 2021, **143**, 11080–11087.
17 N. W. Kabat, E. Monazami and P. Reinke, *Phys. Chem. Chem. Phys.*, 2020, **22**, 26972–26981.
18 K. Walzer, M. Sternberg and M. Hietschold, *Surf. Sci.*, 1998, **415**, 376–384.